Proceedings World Geothermal Congress 2026
Calgary, Canada, June 8 – 11, 2026

From Rock To Geothermal Brine: Insights From Strontium Isotopes In Granite And Sedimentary Rocks Of Soultz-sous-Forêts

David Fries[1]*, Carole Glaas[1], Albert Genter[2]

ÉS-Géothermie, 26 boulevard du Président Wilson, Strasbourg, France[1]*, Genter Geothermal, Menestreau la Villette, France[2]

david.fries@es.fr

Keywords: Strontium isotopes, granite, sedimentary rocks, hydrothermal alteration, geothermal.

ABSTRACT

The origin of elemental enrichment in geothermal brines (e.g. Li, Sr, Mg, B) from deep Upper Rhine Graben (URG) reservoirs is complex, involving multiple lithologies and fault-controlled flow paths. Better understanding the processes driving chemical enrichment in geothermal water could help optimize resource development, particularly if critical raw materials (e.g., lithium) are to be extracted. However, the mechanisms of fluid–rock interaction that led to the current geochemical composition of URG brines remain poorly understood. In this study, strontium isotope ratios ($^{87}Sr/^{86}Sr$) were measured in geothermal fluids, and, in granite and sedimentary rocks from three deep geothermal wells at Soultz-sous-Forêts (GPK-1, GPK-2, EPS-1) in France. Over 50 core samples were analyzed, with $^{87}Sr/^{86}Sr$ ratios ranging from 0.7087 to 0.7863. This wide isotopic variability mainly reflects mineralogical composition but can also indicate progressive water–rock interaction. For instance, in granites affected by argillic alteration, illite formation (which incorporates K and thus ^{87}Rb) can drive $^{87}Sr/^{86}Sr$ ratios towards higher values over time due to radioactive decay. The isotopic similarity between the Soultz-sous-Forêts brine (0.7111 to 0.7116) and fresh monzogranite (0.7087 to 0.7133) suggests that granite may contribute to the Sr content in the brine. However, fractured Triassic sedimentary rocks also show Sr isotopic signatures close to those of the fluids (0.7100 to 0.7317), indicating that fluid–rock interactions extend beyond the granite basement. These findings highlight the role of Sr isotopes as tracers of fluid provenance and hydrothermal alteration in deep geothermal systems.

1 INTRODUCTION

Understanding the origin and evolution of geothermal brines is essential for assessing their potential as secondary sources of critical raw materials. Differentiating the contributions of fluids from various reservoir lithologies is also practical for geothermal applications, as it enables quantification of the relative input from each geological unit to the overall produced fluid. In the Upper Rhine Graben (URG), geothermal fluids typically exhibit total dissolved solid (TDS) concentrations exceeding 100 g/L and are notably enriched in lithium, making them valuable for both energy production and resource evaluation (Sanjuan et al., 2016; Gourcerol et al., 2024). Despite slight variations in salinity, these fluids share a consistent chemical composition dominated by Cl, Na, Ca, and K and display relatively similar isotopic ratios, suggesting a common origin across most geothermal sites in the region (Sanjuan et al., 2016). While extensive geochemical characterization of these fluids were conducted (Sanjuan et al., 2010, 2016; Bosia et al., 2021; Fries et al., 2025), the precise lithological sources and alteration processes contributing to their composition remain insufficiently constrained.

To address this, strontium (Sr) concentrations and isotopic ratios ($^{87}Sr/^{86}Sr$) in the source rocks can be used as geochemical tracers to better understand the origin and evolution of these geothermal fluids. Sr isotopes are particularly valuable because they can reflect the signature of the rocks with which the fluids have equilibrated, making them effective indicators of fluid provenance. Once chemical equilibrium is reached between the fluid and its host rock, further exchange of strontium between the two components becomes limited. As a result, the Sr isotopic composition of the fluid tends to stabilize and no longer evolves significantly, reflecting the dominant mineral contributions established during earlier stages of fluid–rock interaction (Zuddas et al., 1995; Lüders et al., 2010). Importantly, $^{87}Sr/^{86}Sr$ ratios do not fractionate during hydrothermal alteration or fluid–rock interaction, which reinforces their reliability as tracers of lithological sources rather than alteration processes. However, as emphasized by Glodny and Grauert (2009), Sr isotopic signatures in fluids do not necessarily represent the bulk composition of the host rock. Mainly because fluid-rock interaction in polymineralic systems is often mineral selective, meaning that only certain minerals (e.g., biotite or plagioclase) contribute to the Sr budget of the fluid, depending on their solubility and reactivity under hydrothermal conditions. (Zuddas et al., 1995; Aquilina et al., 1997; Glodny and Grauert, 2009). Moreover, ^{87}Rb (rubidium) undergoes radioactive decay to ^{87}Sr over geological

timescales, a process that forms the basis of the Rb–Sr geochronometer and links Sr isotopic compositions to the long-term evolution of geothermal reservoirs (Glodny and Grauert, 2009). Despite this complexity, Sr isotopes remain a powerful tool for tracing fluid-mineral interactions and identifying lithological contributions, especially when combined with geochemical data of both fluids and rocks.

In the URG, geothermal brines collected from the granite basement exhibit $^{87}Sr/^{86}Sr$ ratios between 0.7113 to 0.7116 for Soultz-sous-Forêts (SsF), Insheim and Landau (Aquilina et al., 1997; Millot and Négrel, 2007; Sanjuan et al., 2016). In the Buntsandstein formation, these $^{87}Sr/^{86}Sr$ ratios measured in the fluids are more variable with values going from 0.7098 at Bühl to 0.7118 at Cronenbourg or even higher at Bruchsal with values reaching 0.7150 (Aquilina et al., 1997; Sanjuan et al., 2016). These values are all significantly higher than those of Triassic seawater (0.7068–0.7078) and modern seawater (~0.7091; Burke et al., 1982). The higher $^{87}Sr/^{86}Sr$ in these URG fluids (or in close location like Baden-Baden) suggests that Sr was introduced into the fluids through dissolution of radiogenic minerals, particularly biotite ($^{87}Sr/^{86}Sr$ = ~2.6646) at lower temperature and plagioclase or K-feldspar ($^{87}Sr/^{86}Sr$ = 0.7074 for plagioclase and 0.7111-0.716 for K-feldspar) at higher temperature (Aquilina et al., 1997; Sanjuan et al., 2016; Stober et al., 2025). Two distinct isotopic trends were identified, one reflecting widespread biotite dissolution common to both lithologies (Buntsandstein and monzogranite), and another specific to plagioclase dissolution within the monzogranite.

While geothermal fluid compositions in the URG were characterized in several locations, the Sr isotopic composition of the reservoir rocks themselves remains underexplored. Existing measurements of $^{87}Sr/^{86}Sr$ in Buntsandstein and Muschelkalk formations are relatively limited. Ploquin (2011) measured in core rock samples, in the Paris Basin, $^{87}Sr/^{86}Sr$ values that are comprised between 0.7118 and 0.7315 for the Buntsandstein formation (n = 5) and 0.7120 and 0.7353 for the Muschelkalk formation (n = 3). Similarly, while the crystalline basement was studied for its geochemistry (Genter, 1989; Dugamin et al., 2024; Jungmann et al., 2025; Fries et al., 2025), its Sr isotopic variability across different alteration facies remains poorly constrained. Monzogranite samples from the SsF EPS-1 and GPK-1 wells, collected at 1,820 and 1,995 m depth respectively, have $^{87}Sr/^{86}Sr$ values ranging from 0.7100 to 0.7111 (Zuddas et al., 1995; Cocherie et al., 2004). These ratios are lower than SsF fine-grained two-mica granite sampled at 5,058 m depth with a more radiogenic $^{87}Sr/^{86}Sr$ ratio of 0.7173 (Cocherie et al., 2004).

This study presents new measurements of $^{87}Sr/^{86}Sr$ ratios in core rock samples from the crystalline monzogranite basement, the Buntsandstein sandstones, and the Muschelkalk carbonates. Particular attention is given to the Sr isotopic signature of various alteration facies within the monzogranite, aiming to better understand the sources and evolution of Sr in geothermal fluids. These data provide a new baseline for interpreting fluid-rock interactions and tracing the origin of geothermal brines in the URG.

2 STUDY AREA AND SAMPLE DESCRIPTION

The SsF site is in the Western part of the URG, which is a Cenozoic rift structure showing a series of thermal anomalies characterized by a thermal gradient up to 100°C/km (Haas and Hoffmann, 1929). Many former petroleum fields are superimposed to those thermal anomalies which are interpreted as the trace of natural brine advection inside a nearly vertical fracture system cross-cutting both deep-seated Triassic sediments and Palaeozoic crystalline basement (Genter et al., 2010). The SsF geothermal wells were implanted on a local horst structure bounded by faults showing an apparent normal off-set of 500 m (Figure 1). A sedimentary pile of 1,400 m thick is made of Cenozoic marine and lacustrine limestones, marls and evaporites, including the petroleum layers of Pechelbronn, overlaying in unconformity the Jurassic limestones and the Triassic formations made of Keuper marl and evaporite, Muschelkalk limestone and Buntsandstein sandstone. These Cenozoic and Mesozoic sediments were deposited in unconformity on the Palaeozoic basement, which includes a porphyritic monzogranite and a fine-grained two-mica granite. Natural permeability was systematically observed in fractured zones/faulted zones in the crystalline basement which was significantly improved by applying various stimulation techniques (Schill et al., 2017). Three geothermal wells (GPK-2, GPK-3, and GPK-4), drilled from the same platform, reached depths of about 5,000 m. Prior to these deep exploitation wells, two exploration wells, GPK-1 and EPS-1,were drilled to 3,600 m and 2,230 m, respectively, and were partly to fully cored (Genter et al., 2010). Approximately 50 m of spot cores were recovered from GPK-1, while EPS-1 yielded about 1,300 m of continuous cores. In GPK-2, only a single core of ~1 m was obtained from the deep granite at 5,058 m depth. For this study, available core samples from Triassic sedimentary formations and the Paleozoic crystalline granites collected in GPK-1, GPK-2, and EPS-1 were analyzed (Figure 1).

The samples selected for this study are described in detail in Fries et al. (2025) for the deep-seated fractured crystalline rocks and Glaas et al. (2025) for the deep-seated sedimentary rocks. These previous studies conducted a geochemical characterization of both crystalline and sedimentary reservoir rocks from the Soultz-

sous-Forêts geothermal site, using core rock samples collected between 841 and 5,058 m depth from wells GPK-1, GPK-2, and EPS-1. Similarly, this study uses the same sample collection but focuses on Sr isotopes analyses. A total of 56 samples were analyzed in this study including 36 samples collected in the crystalline basement and 20 samples from the sedimentary reservoir (Figure 1).

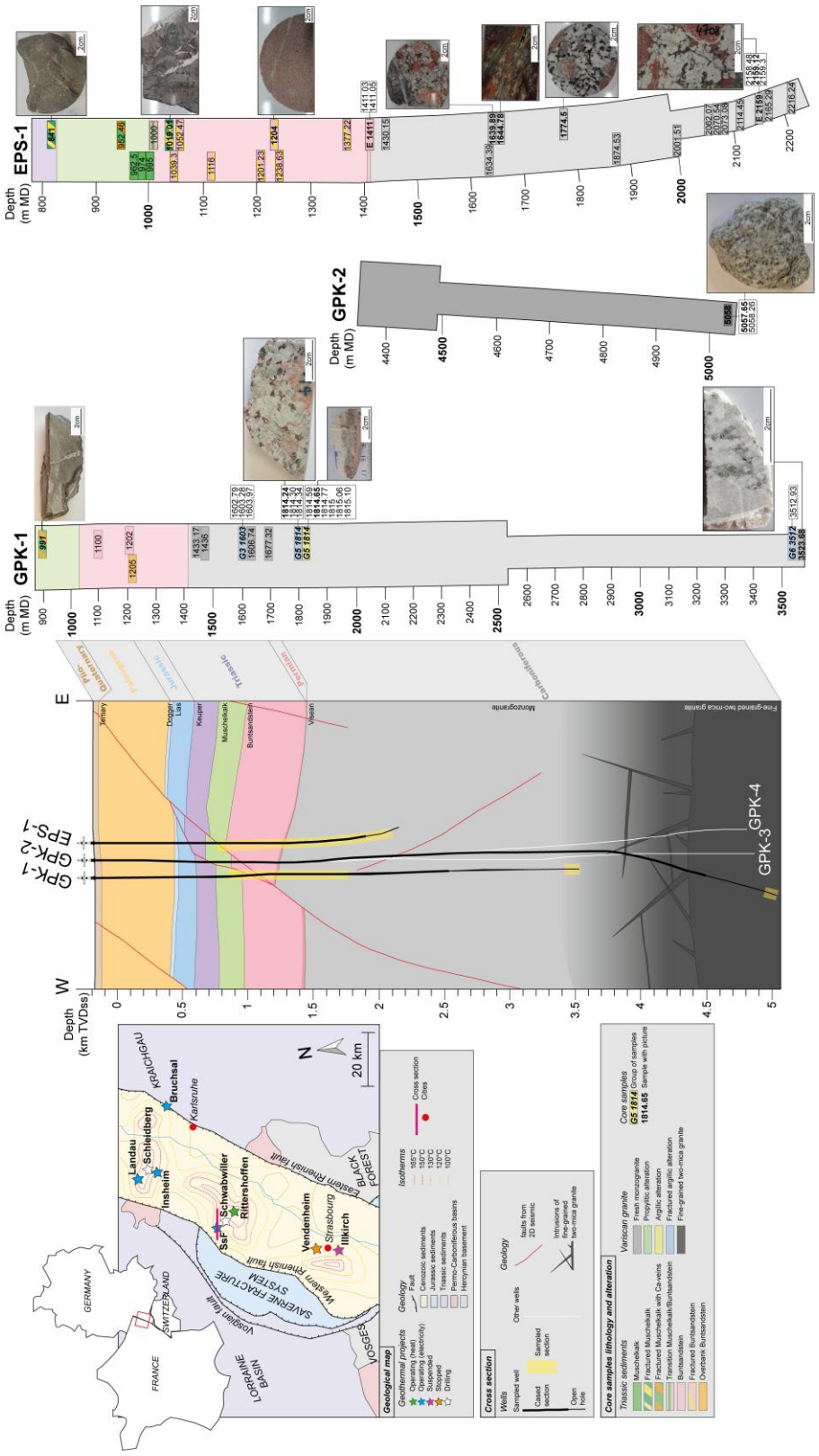


Figure 1. Schematic geological map of the Upper Rhine Graben showing the geothermal site locations (Glaas, 2021). Interpreted geological cross-section showing the Soultz-sous-Forêts (SsF) geothermal wells trajectories which are projected along the W-E axis. Locations of the core samples taken along the borehole trajectories that were analyzed for geochemical characterization (on the right).

All the granitic rock samples were selected to ensure that each granite type was sufficiently represented to allow statistical analyses on each facies: 6 samples of fresh granite (4 monzogranites and 2 fine-grained two-mica granites), 4 samples in the propylitic alteration, 11 samples in the argillic alteration and 11 samples in the fractured argillic alteration. Additionally, within hydrothermally altered facies, 3 samples in the tosudite occurrence zone and 1 sample where kaolinite was identified were also collected for this study. Sedimentary rock samples were collected to represent the full range of mineralogical changes throughout the entire thickness of the Triassic sedimentary sequence: 3 for the Muschelkalk, 2 for the fractured Muschelkalk, 2 for the fractured Muschelkalk with Ca-veins, 1 for the transition between Muschelkalk and Buntsandstein, 4 for the Buntsandstein, 7 for the fractured Buntsandstein, and 1 for the overbanks in the Buntsandstein.

3 MATERIALS AND METHODS

The geochemical analyses for the selected rock samples were carried out at the Service d'Analyse des Roches et des Minéraux (SARM) of the Centre de Recherches Pétrographiques et Géochimiques (CRPG) in Nancy, France. Before analyses, all the rock samples were grinded to reach a particle size of solid samples lesser than 80 µm. Major, minor, and trace element concentrations in rock samples were determined following alkaline fusion with lithium metaborate ($LiBO_2$) at 1,000 °C for 60 minutes. The resulting melts were dissolved in a reagent mixture of HNO_3 (1 mol/L), H_2O_2 (~0.5 v/v), and glycerol (~10% v/v), following the protocol of Carignan et al. (2001). Ba, Sr, and Rb concentrations were quantified by inductively coupled plasma mass spectrometry (ICP-MS, Thermo ICAP Q). Analytical uncertainties depend on concentration levels, for Sr and Rb all the uncertainties are <10%.

Sr ratio measurements were carried out by SEDISOR. Approximately 300 mg of powdered sample were digested in Savillex® beakers using a mixture of ultrapure HF (2 mL, 24 N), HNO_3 (3 mL, 14 N), and bidistilled $HClO_4$ (0.5 mL, 10 N) at 120 °C for 72 h. After evaporation to dryness at 180 °C, residues were treated with aqua regia for 24 h at 110 °C, then dissolved in 15 mL of 6 N HCl to prepare the mother solution. Aliquots of the mother solution were evaporated to dryness, converted to nitrate with concentrated HNO_3, and redissolved in 1 mL of 1 N HNO_3. After centrifugation, samples were loaded onto Biorad® columns with Triskem® Sr-SPEC resin for Sr separation from the matrix (Pin and Zalduegui, 1997; Révillon et al., 2011). Sr was eluted in 2 mL of hot ultrapure water.

Isotopic measurements were performed at the Pôle de Spectrométrie Océan (PSO), in Brest, France. Samples were loaded on W filaments with Ta activator for thermal ion mass spectrometer (TIMS) measurements. Sr isotope compositions were measured in static mode on a Thermo TRITON at the PSO. Sr isotope compositions of standard solution NBS987 gave $^{87}Sr/^{86}Sr = 0.710259 \pm 0.000005$ (2σ, n = 8), consistent with the recommended value (0.710250), with external reproducibility of ~10 ppm. Procedural blanks were ≤111 pg and considered negligible.

4 RESULTS AND DISCUSSION

4.1 Sr and Rb concentration and behavior in the alteration facies of the granite

Sr and Rb concentration of the sampled granite rocks are displayed in Figure 2. Alteration-related changes in total rock chemical composition are documented in Fries et al. (2025). In the fresh monzogranite, strontium concentrations ([Sr]) range from 384 to 742 ppm (median at 468 ppm), while rubidium concentrations ([Rb]) vary from 167 to 284 ppm (median at 186 ppm). In contrast, the fine-grained two-mica granites exhibit lower [Sr] median value of 259 ppm but slightly higher [Rb] with a median of 202 ppm. Similar results were observed in Cocherie et al. (2004) with the same granite facies. Overall, the highest concentrations of Sr are found in feldspar (plagioclase and K-feldspar) while the highest concentration of Rb are found in feldspar, muscovite and biotite minerals within the granite (Aquilina et al., 1997; Stussi et al., 2002; Drüppel et al., 2020; Dugamin et al., 2024). Given the chemical differences between the fine-grained two-mica granite and the porphyritic monzogranite, and to better characterize the hydrothermal alteration gradient at comparable depths (as fine-grained samples were only available at 5,058 m), the monzogranite composition is used as the fresh granite reference for comparison. The monzogranites impacted by propylitic alteration (low fluid-rock interaction) display lower Sr (median at 349 ppm) and slightly lower Rb (median at 166 ppm). The decrease in both Sr and Rb concentrations reflects the mineralogical transformation of fresh monzogranite during hydrothermal alteration. Sr depletion is primarily associated with the albitization of calcic plagioclase (oligoclase) and other Sr-rich phases, while biotite alteration to chlorite releases Rb into the geothermal fluid. In monzogranites affected by argillic alteration (fractured or not), Sr concentrations reach their lowest median values (118 ppm in argillic alteration and 58 ppm in fractured argillic alteration; Figure 2), confirming significant Sr loss during fluid–rock interaction. Dugamin et al. (2024) reported that newly formed minerals such as illite contain Sr at concentrations an order of magnitude lower than feldspar, which contributes to the overall Sr depletion observed in altered monzogranites. Although

secondary phases like carbonates (e.g. calcite) or sulfates (e.g. barite) can locally concentrate Sr (Dugamin et al., 2024), their occurrence is limited compared to the widespread formation of low-Sr clays. However, this explains the exceptionally high Sr value (1,225 ppm; Figure 2) in one fractured argillic sample, linked to a barite vein. In contrast, Rb shows an opposite trend, with a global enrichment in the most altered monzogranites (Figure 2). However, [Rb] is more variable, indicating a more complex pattern than [Sr]. Rb enrichment could be attributed to illite formation with high [Rb] (Dugamin et al., 2024), consistent with previous observations in these altered granites that contain a significant proportion of illite (Genter, 1989; Glaas et al., 2021). Therefore, variability in [Rb] may reflect differences in illite abundance. Additionally, Drüppel et al. (2020) highlighted additional Rb hosted in drusy quartz with abundant fluid inclusions, which could explain the higher variability in fractured and altered monzogranites compared to non-fractured and altered samples. Granites containing tosudite and kaolinite also exhibit elevated Rb and reduced Sr, further emphasizing the higher mobility of Sr relative to Rb during hydrothermal alteration.

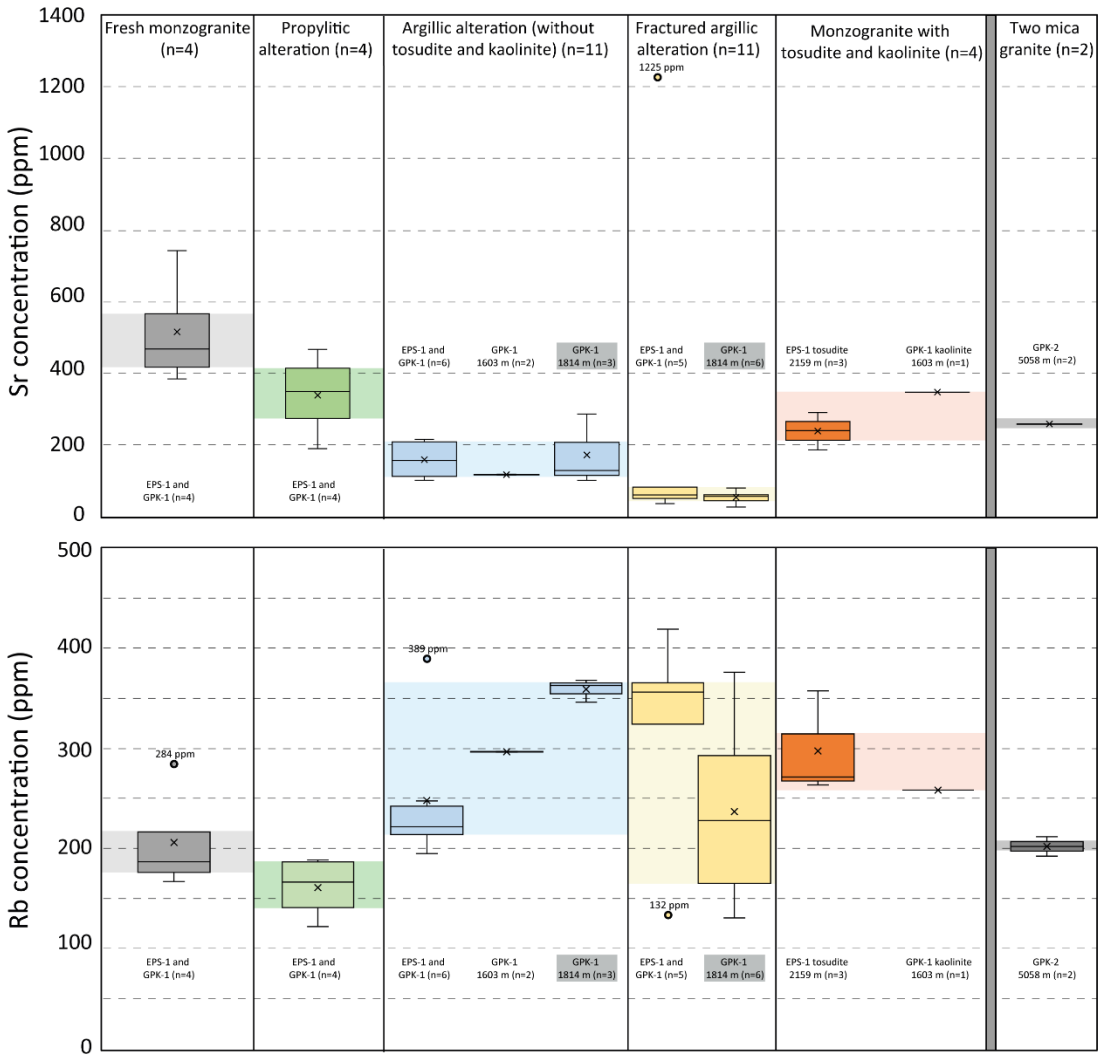


Figure 2. These boxplot diagrams illustrate the distribution of [Sr] and [Rb] in the whole rocks across the different granite alteration facies identified in this study. Several zones in the different wells are described below the boxes. The boxes represent the interquartile range (IQR), encompassing the middle 50% of the data. The horizontal line within the boxes indicates the median concentration, and the cross indicates the average concentration. Whiskers extend to the smallest and largest values within 1.5 times the IQR from the lower and upper quartiles, respectively. Points plotted outside the whiskers highlight outliers beyond these limits.

4.2 Sr and Rb concentration and behavior in the sedimentary formations

Sr and Rb concentration of the sampled sedimentary rocks are displayed in Figure 3. Chemical variations of major elements of the different geological sedimentary formations are also described in Glaas et al. (2025). Similar to granite rocks, the distinct facies of sedimentary rocks were selected based on their physical characteristics of the rocks, particularly focusing on the presence or absence of natural fractures. In

Buntsandstein rocks, [Sr] range from 57 to 88 ppm in non-fractured samples and from 95 to 733 ppm in fractured samples (Figure 3). The enrichment of Sr in fractured Buntsandstein rocks is associated with the presence of barite veins, as indicated by higher barium (Ba) concentrations (median value of 5443 ppm in fractured samples compared to 510 ppm in non-fractured samples; Table 1). A similar trend is observed in Muschelkalk rocks (Figure 3), where fractured samples exhibit higher [Sr] (154 to 977 ppm) than non-fractured samples (66 to 99 ppm). However, Ba concentrations do not differ significantly in these samples (Table 1), suggesting that barite precipitation is not responsible for the [Sr] increase. Instead, an unidentified component in the major chemical analyses (Glaas et al., 2025) suggests that carbonates or other sulfate minerals (e.g., $CaSO_4$, $MgSO_4$, $SrSO_4$) drive Sr enrichment in fractured Muschelkalk rocks. Indeed, newly formed anhydrite minerals were measured with the highest [Sr] just below barite minerals (Dugamin et al., 2024).

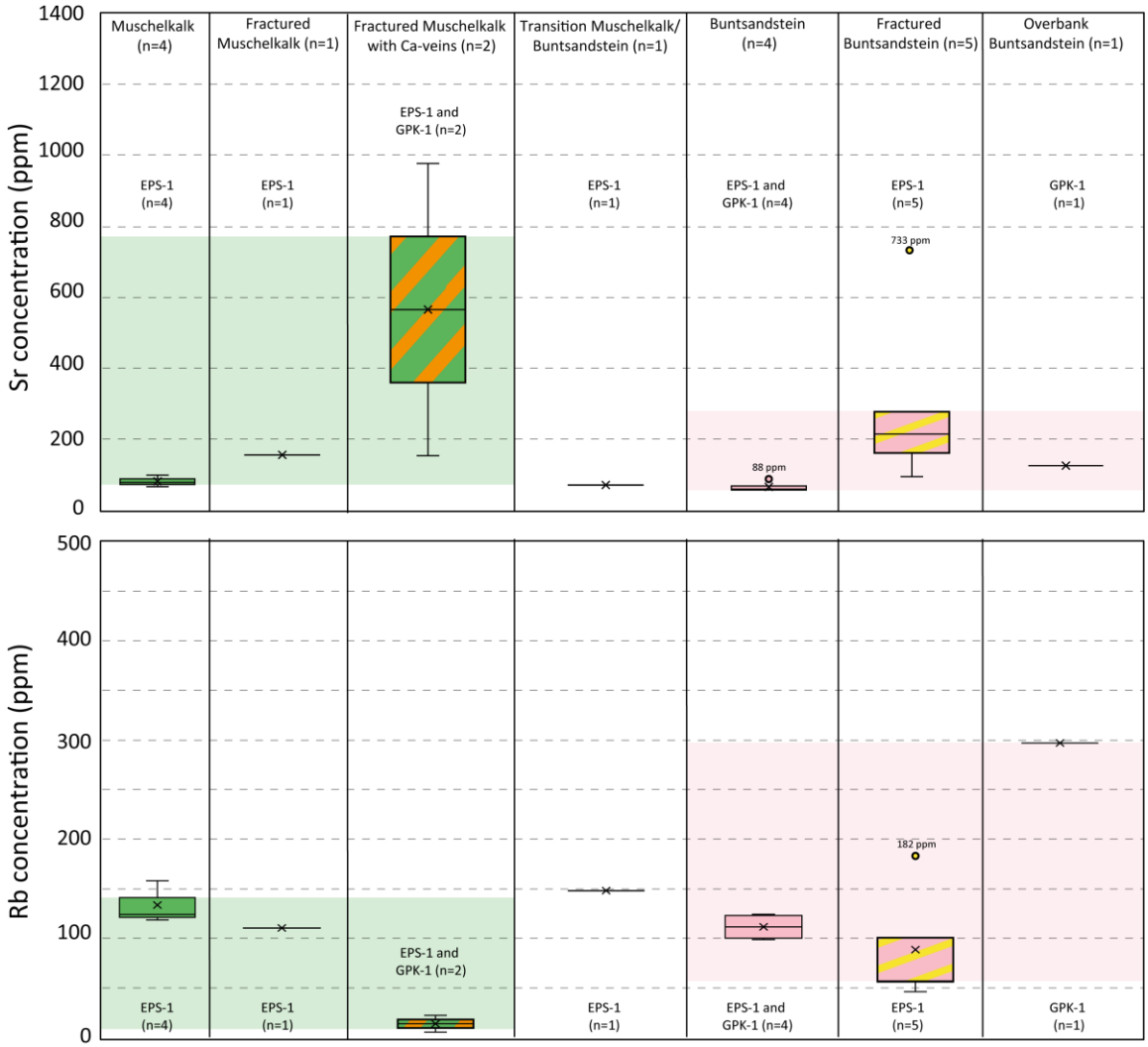


Figure 3. These boxplot diagrams illustrate the distribution of [Sr] and [Rb] in the Muschelkalk and the Buntsandstein sedimentary rocks (fractured or not) identified in this study. Several zones in the different wells are described below the boxes. The boxes represent the interquartile range (IQR), encompassing the middle 50% of the data. The horizontal line within the boxes indicates the median concentration, and the cross indicates the average concentration. Whiskers extend to the smallest and largest values within 1.5 times the IQR from the lower and upper quartiles, respectively. Points plotted outside the whiskers highlight outliers beyond these limits.

The core sample collected at the Muschelkalk/Buntsandstein transition and the overbank Buntsandstein sample exhibit a relatively similar chemical composition, characterized by higher clay content (Glaas et al., 2025). These samples display low [Sr] but the highest [Rb] compared to other sedimentary rocks (Figure 3). This pattern is comparable to highly altered and fractured monzogranite samples, which also contain the highest clay content and consequently the highest Rb concentrations. Globally, fractured sedimentary rocks show lower [Rb] than non-fractured rocks. In fractured Muschelkalk rocks, this decrease in Rb is attributed to the presence of abundant carbonate veins, which dilute [Rb] due to the increase in total elemental content and the limited

mobility of Rb. In fractured Buntsandstein rocks, the lower Rb concentrations may reflect either a reduced abundance of Rb-bearing minerals (biotite, muscovite, or feldspar) or lower clay content compared to non-fractured Buntsandstein rocks. One sample from EPS-1 (1,039.3 m) contains 182 ppm Rb (the highest value measured for this facies) along with the highest Al_2O_3 content (11.1 %) and is located in a zone with elevated gamma-ray indicating clay presence (Glaas et al., 2025). The variability of Rb in Buntsandstein rocks also appears to be linked to clay content, primarily illite, which can host significant Rb, as demonstrated by Dugamin et al. (2024).

Table 1. Median barium concentrations ([Ba]) in monzogranite, Muschelkalk, and Buntsandstein sedimentary rocks

	Rock type	[Ba] median (ppm)
Monzogranite	Fresh monzogranite	1025
	Propylitic alteration	330
	Argillic alteration	366
	Fractured and argillic alteration	547
Sedimentary	Muschelkalk	182
	Fractured Muschelkalk	124
	Fractured Muschelkalk with Ca-veins	101
	Buntsandstein	510
	Fractured Buntsandstein	5443

4.3 Strontium isotope signatures of the geothermal reservoir

The Sr isotopic composition of the monzogranite core samples, regardless of their alteration state, is highly variable with $^{87}Sr/^{86}Sr$ ratios between 0.7087 and 0.7863 (Figure 4). The fresh monzogranite and the propylitic altered monzogranite (the less altered rocks) have Sr isotopic composition (0.7087-0.7133) in the same range than previous measurements (Zuddas et al., 1995; Cocherie et al., 2004) but also than modern measurement of the SsF geothermal water. The Sr isotopic composition of the SsF geothermal brine (0.7113-0.7116) closely matches that of the fresh monzogranite (median at 0.7122), indicating significant interaction and likely equilibrium with this rock. Hydrothermal alteration resulted in a clear Sr loss (Figure 3), highlighting the monzogranite's contribution to the brine Sr budget and its isotopic signature.

In contrast, the sedimentary cover exhibits less variability: Buntsandstein rocks (fractured and non-fractured) range from 0.7120 to 0.7317, while Muschelkalk rocks (fractured and non-fractured) range from 0.7100 to 0.7274. These variations, similar to previous observations (Ploquin, 2011), likely reflect diagenetic processes and fluid–rock interactions that influence the Rb–Sr system. For example, Sr gain through calcite precipitation can lower $^{87}Sr/^{86}Sr$ ratios, as calcite veins with a hydrothermal origin typically exhibit values of 0.7088 to 0.7108 (Glodny and Grauert, 2009), explaining the lower ratios in fractured Muschelkalk rocks. Similarly, fractured Buntsandstein rocks show decreased ratios due to the presence of barite veins, which tend to have ratios around 0.710 to 0.714 (Permian barite; Staude et al., 2011). These $^{87}Sr/^{86}Sr$ ratios are very close to those of the geothermal fluid (Figure 4), indicating that these newly formed mineral in the sedimentary rocks could record the Sr isotopic signature of the circulating brine at the time, which originated from interaction with the monzogranite. Furthermore, barite or calcite incorporates negligible Rb compared to Sr (Dugamin et al., 2024) and therefore cannot significantly change the Sr composition of barite over time (Staude et al., 2011).

In both monzogranite and sedimentary rocks, clay minerals enriched in Rb drive ratios toward higher values. Highly altered and fractured granite exhibits the highest ratios, suggesting that illite presence increases $^{87}Sr/^{86}Sr$ and that hydrothermal alteration can be detected using Sr isotopes. In the monzogranite, the greater variability of $^{87}Sr/^{86}Sr$ ratios in fractured and argillic granite compared to the argillic granite (Figure 4) could also be influenced by newly formed minerals such as barite, which can affect the $^{87}Sr/^{86}Sr$ ratios.

Interestingly, the highest Rb and $^{87}Sr/^{86}Sr$ ratios in non-fractured Muschelkalk and Buntsandstein rocks could indicate higher clay content, resulting from diagenesis or hydrothermal alteration.

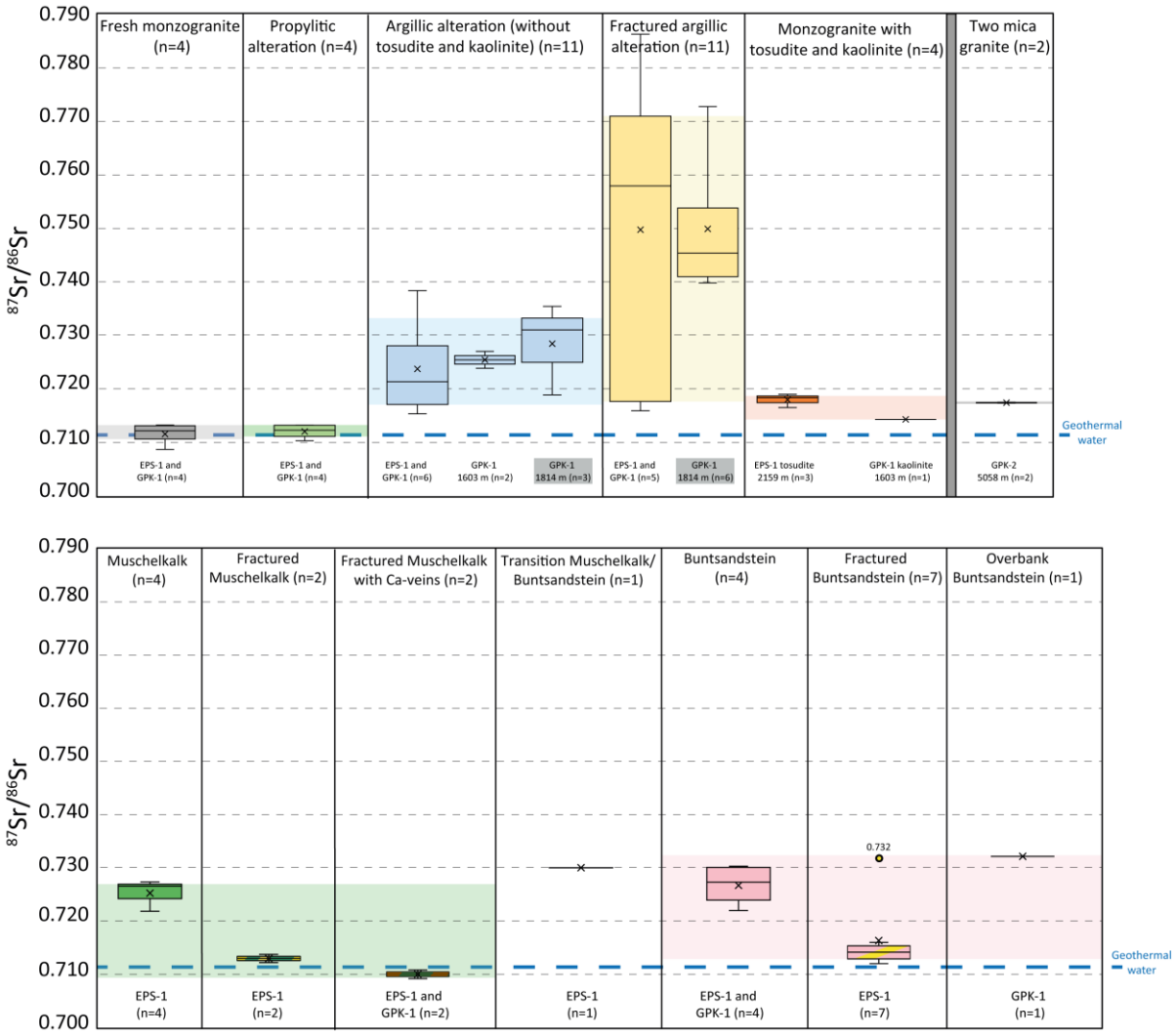


Figure 4. These boxplot diagrams illustrate the distribution of $^{87}Sr/^{86}Sr$ in the monzogranite and its different alteration facies and in the Muschelkalk and the Buntsandstein sedimentary rocks (fractured or not) identified in this study. Several zones in the different wells are described below the boxes. The boxes represent the interquartile range (IQR), encompassing the middle 50% of the data. The horizontal line within the boxes indicates the median concentration, and the cross indicates the average concentration. Whiskers extend to the smallest and largest values within 1.5 times the IQR from the lower and upper quartiles, respectively. Points plotted outside the whiskers highlight outliers beyond these limits. The blue dashed line represents the $^{87}Sr/^{86}Sr$ measured in the geothermal fluid of Soultz-sous-Forêts (0.7113-0.7116).

5 CONCLUSION

The Sr isotopic composition of the SsF geothermal brine strongly indicates interaction with the deep monzogranite, whose $^{87}Sr/^{86}Sr$ ratios closely match those of the brine, identifying this monzogranite as a major source of Sr. Sr isotopes also provide a tool for characterizing past hydrothermal alteration, as elevated $^{87}Sr/^{86}Sr$ ratios are associated with clay-rich zones and intense alteration processes. Precipitation of minerals such as calcite, barite, or anhydrite controls most of the Sr budget in sedimentary rocks and therefore drives their Sr isotopic composition. These minerals often preserve the Sr isotopic signature of the circulating brine at the time of their formation, which closely matches the geothermal fluid and reflects its origin from interaction with the monzogranite.

Additionally, this approach offers potential for estimating the timing of the last fluid–rock interactions. Future research should integrate Sr isotopic data with other isotope systems, such as Li isotopes, to validate lithium sources and better characterize element mobility in deep geothermal reservoirs of the Upper Rhine Graben.

Acknowledgements

This project research, LICORNE, was funded by the European Union under Grant Agreement No 101069644. Views and opinions expressed are, however, those of the authors only and do not necessarily reflect those of the European Union or the European Climate, Infrastructure and Environment Executive Agency (CINEA). Neither the European Union nor the granting authority can be held responsible for them. The authors are grateful to GEIE Exploitation Minière de la Chaleur for accessing the cores at the Soultz-sous-Forêts geothermal site. The authors are also grateful to the technical team of ÉS-Géothermie operating the Soultz power plant for their assistance during fluid and rock sampling, especially for their preparation.

REFERENCES

Aquilina L., Pauwels H., Genter A. and Fouillac C. (1997) Water-rock interaction processes in the Triassic sandstone and the granitic basement of the Rhine Graben: Geochemical investigation of a geothermal reservoir. *Geochim. Cosmochim. Acta* **61**, 4281–4295.

Bosia C., Mouchot J., Ravier G., Seibt A., Jähnichen S., Degering D., Scheiber J., Baujard C. and Genter A. (2021) Evolution of brine geochemical composition during operation of EGS geothermal plants (Alsace, France). In *Proceedings, 46th Workshop on Geothermal Reservoir Engineering, 16-18 February 2021* Stanford University, California, USA. p. 21.

Burke W. H., Denison R. E., Hetherington E. A., Koepnick R. B., Nelson H. F. and Otto J. B. (1982) Variation of seawater 87Sr/86Sr throughout Phanerozoic time. *Geology* **10**, 516–519.

Carignan J., Hild P., Mevelle G., Morel J. and Yeghicheyan D. (2001) Routine analyses of trace elements in geological samples using flow injection and low pressure on-line liquid chromatography coupled to ICP-MS: a study of geochemical reference materials BR, DR-N, UB-N, AN-G and GH. *Geostand. Newsl.* **25**, 187–198.

Cocherie A., Guerrot C., Fanning C. M. and Genter A. (2004) Datation U–Pb des deux faciès du granite de Soultz (Fossé rhénan, France). *C. R.-Geosci.* **336**, 775–787.

Drüppel K., Stober I., Grimmer J. C. and Mertz-Kraus R. (2020) Experimental alteration of granitic rocks: Implications for the evolution of geothermal brines in the Upper Rhine Graben, Germany. *Geothermics* **88**, 101903.

Dugamin E. J. M., Boiron M.-C., Cathelineau M., Richard A., Peiffert C., Lebreton A., Banks D. A. and Despinois F. (2024) Brine-granite interaction and lithium leaching in a continental rift (Soultz-sous-Forêts, Rhine Graben, France). *Lithos* **478–479**, 107604.

Fries D., Glaas C. and Genter A. (2025) Hydrothermal alteration role on lithium mobility in a geothermal reservoir: Geochemical analyses of deep granite in the Upper Rhine Graben. In *Proceedings, 50th Workshop on Geothermal Reservoir Engineering, 10-12 February 2025* Stanford University, California, USA.

Genter A. (1989) Géothermie roches chaudes sèches: le granite de Soultz-sous-Forêts (Bas-Rhin, France): fracturation naturelle, altérations hydrothermales et interaction eau-roche. PhD Thesis, Université d'Orléans.

Genter A., Evans K., Cuenot N., Fritsch D. and Sanjuan B. (2010) Contribution of the exploration of deep crystalline fractured reservoir of Soultz to the knowledge of enhanced geothermal systems (EGS). *C. R.-Geosci.* **342**, 502–516.

Glaas C. (2021) Mineralogical and structural controls on permeability of deep naturally fractured crystalline reservoirs Insights from geothermal wells (Upper Rhine Graben). PhD Thesis, Université de Strasbourg.

Glaas C., Fries D., Rumbach G. and Genter A. (2025) Geochemical analyses of Triassic rocks in the Upper Rhine Graben: A first lithium study in sedimentary rocks of Soultz-sous-Forêts wells. In *European Geothermal Congress 2025, 06-10 October 2025* Zurich, Switzerland.

Glaas C., Patrier P., Vidal J., Beaufort D. and Genter A. (2021) Clay Mineralogy: A Signature of Granitic Geothermal Reservoirs of the Central Upper Rhine Graben. *Minerals* **11**, 479.

Glodny J. and Grauert B. (2009) Evolution of a hydrothermal fluid-rock interaction system as recorded by Sr isotopes: A case study from the Schwarzwald, SW Germany. *Mineralogy and Petrology* **95**, 163–178.

Gourcerol B., Sanjuan B., Millot R., Rettenmaier D., Jeandel E., Genter A., Bosia C. and Rombaut A. (2024) Atlas of lithium geothermal fluids in Europe. *Geothermics* **119**, 102956.

Haas I. O. and Hoffmann C. R. (1929) Temperature gradient in Pechelbronn oil bearing region, lower Alsace: its determination and relation to oil reserves. *Bull. Am. Assoc. Pet. Geol.* **13**, 1257–1273.

Jungmann M., Walter B. F., Eiche E., Giebel R. J. and Kolb J. (2025) The source of lithium in connate fluids: Evidence from the geothermal reservoir at Soultz-sous-Forêts, Upper Rhine Graben, France. *J. Geochem. Explor.* **270**, 107641.

Lüders V., Plessen B., Romer R. L., Weise S. M., Banks D. A., Hoth P., Dulski P. and Schettler G. (2010) Chemistry and isotopic composition of Rotliegend and Upper Carboniferous formation waters from the North German Basin. *Chemical Geology* **276**, 198–208.

Millot R. and Négrel P. (2007) Multi-isotopic tracing (δ7Li, δ11B, 87Sr/86Sr) and chemical geothermometry: evidence from hydro-geothermal systems in France. *Chem Geol* **244**, 664–678.

Pin C. and Zalduegui J. S. (1997) Sequential separation of light rare-earth elements, thorium and uranium by miniaturized extraction chromatography: Application to isotopic analyses of silicate rocks. *Analytica Chimica Acta* **339**, 79–89.

Ploquin F. (2011) Argiles, traceurs de paléoconditions diagénétiques et hydrothermales. Université de Poitiers. UFR des sciences fondamentales et appliquées, France.

Révillon S., Jouet G., Bayon G., Rabineau M., Dennielou B., Hémond C. and Berné S. (2011) The provenance of sediments in the Gulf of Lions, western Mediterranean Sea. *Geochemistry, Geophysics, Geosystems* **12**.

Sanjuan B., Millot R., Dezayes C. and Brach M. (2010) Main characteristics of the deep geothermal brine (5 km) at Soultz-sous-Forêts (France) determined using geochemical and tracer test data. *C. R.-Geosci.* **342**, 546–559.

Sanjuan B., Millot R., Innocent Ch., Dezayes Ch., Scheiber J. and Brach M. (2016) Major geochemical characteristics of geothermal brines from the Upper Rhine Graben granitic basement with constraints on temperature and circulation. *Chem. Geol.* **428**, 27–47.

Schill E., Genter A., Cuenot N. and Kohl T. (2017) Hydraulic performance history at the Soultz EGS reservoirs from stimulation and long-term circulation tests. *Geothermics* **70**, 110–124.

Staude S., Göb S., Pfaff K., Ströbele F., Premo W. R. and Markl G. (2011) Deciphering fluid sources of hydrothermal systems: A combined Sr- and S-isotope study on barite (Schwarzwald, SW Germany). *Chem Geol* **286**, 1–20.

Stober I., Grimmer J. C. and Kraml M. (2025) Origin and development of the geothermal fluids of the Baden-Baden area (SW-Germany): implications for geothermal systems of granitic reservoirs. *Swiss Journal of Geosciences* **118**, 8.

Stussi J.-M., Cheilletz A., Royer J.-J., Chèvremont P. and Féraud G. (2002) The hidden monzogranite of Soultz-sous-Forêts (Rhine Graben, France). Mineralogy, petrology and genesis. *Geol. Fr.* **1**, 45–64.

Zuddas P., Seimbille F. and Michard G. (1995) Granite-fluid interaction at near-equilibrium conditions: Experimental and theoretical constraints from Sr contents and isotopic ratios. *Chem Geol* **121**, 145–154.